BASIC SCIENCE

Nanomedicine: Nanotechnology, Biology, and Medicine
44 (2022) 102577

Original Article

nanomedjournal.com

Development of a SERS based cancer diagnosis approach employing cryosectioned thyroid tissue samples on PDMS

Sevda Mert, Ph.D.[a,b], Seda Sancak, M.D.[c], Hasan Aydın, M.D.[d], Ayşe Tuba Fersahoğlu, M.D.[e], Adnan Somay, M.D.[f], Ferda Özkan, M.D.[g], Mustafa Çulha, P.hD.[h,i,j,*]

[a]*Department of Genetics and Bioengineering, Faculty of Engineering, Yeditepe University, Istanbul 34755, Turkey*
[b]*Department of Genetics and Bioengineering, Faculty of Engineering, Istanbul Okan University, Istanbul 34959, Turkey*
[c]*Department of Internal Medicine, Endocrinology and Metabolism Disorders, Fatih Sultan Mehmet Education and Research Hospital, University of Health Sciences, Istanbul 34752, Turkey*
[d]*Department of Internal Medicine, Section of Endocrinology and Metabolism, Yeditepe University Hospital, Istanbul 34752, Turkey*
[e]*General Surgery Clinic, Fatih Sultan Mehmet Education and Research Hospital, University of Health Sciences, Istanbul 34752, Turkey*
[f]*Department of Pathology, Fatih Sultan Mehmet Education and Research Hospital, University of Health Sciences, Istanbul 34752, Turkey*
[g]*Department of Pathology, Yeditepe University Hospital, Istanbul 34752, Turkey*
[h]*The Knight Cancer Institute, Cancer Early Detection Advanced Research Center (CEDAR), Oregon Health and Science University, Portland 97239, OR, USA*
[i]*Sabanci University Nanotechnology Research and Application Center (SUNUM), Tuzla, Istanbul 34956, Turkey*
[j]*Department of Chemistry & Physics, Augusta University, Augusta, GA 30912, USA*

Revised 30 May 2022

Abstract

An efficient SERS based novel analytical approach named Cryosectioned-PDMS was developed systematically and evaluated applying on 64 thyroid biopsy samples. To utilize thyroid biopsy samples, a 20-μl volume of h-AgNPs suspension was dropped on a 5-μm thick cryosectioned biopsy specimen placed on the PDMS coated glass slide. The SERS spectra from a 10 × 10 points array acquired by mapping 22.5 μm × 22.5 μm sized area from suspended dried droplets placed on the tissue surface. The probability of correctly predicted performance for diagnosis of malignant, benign and healthy tissues was resulted in the accuracy of 100 % for the spectral bands at 667, 724, 920, 960, 1052, 1096, 1315 and 1457 cm^{-1} using PCA-fed LDA machine learning. The Cryosectioned-PDMS biophotonic approach with PCA-LDA predictive model demonstrated that the vibrational signatures can accurately recognize the fingerprint of cancer pathology from a healthy one with a simple and fast sample preparation methodology.
© 2022 Elsevier Inc. All rights reserved.

Keywords: Surface-enhanced Raman scattering biosensor; Cancer diagnosis; Cryosectioned-polydimethylsiloxane approach; Principle component analysis; Linear discriminant analysis

Background

Cancer continues to be the leading cause of death in the developing world although it is currently overshadowed by the COVID-19 pandemic. Thyroid cancer is one of the cancer types having a rapid increase in incidence, especially in young people.[1] The status of focal thyroid lesions during diagnosis is one of the most debated issues between endocrinologists and surgeons. The gold standard for the identification and therapeutic process of thyroid lesions is generally based on high-resolution ultrasonography (US) and fine-needle aspiration cytology (FNAC). The pathological examination of 7 to 16 % abnormal thyroid tissue results in a malignant diagnosis possessing sensitivity and specificity of 83 to 98 % and 70 to 92 %, respectively.[2,3] Papillary thyroid carcinoma (PTC) is the most common cancer type of thyroid cancer cases with an occurrence range of 70 to 80 %. The other types are follicular thyroid carcinoma (FTC), medullary thyroid carcinoma (MTC) and anaplastic thyroid cancer with an occurrence range of 15 to 20 %, 5 to 10 % and 2 to 5 %, respectively.[4,5] From its diagnosis to treatment, several challenges are still intact, and it requires a truly multidisciplinary approach. The success in cancer treatment starts with

* Corresponding author at: Department of Chemistry & Physics, Augusta University, Augusta, GA 30912, USA.
E-mail address: mustafa.culha@sabanciuniv.edu (M. Çulha).

https://doi.org/10.1016/j.nano.2022.102577
1549-9634/© 2022 Elsevier Inc. All rights reserved.

Please cite this article as: Mert S, et al, Development of a SERS based cancer diagnosis approach employing cryosectioned thyroid tissue samples on PDMS. *Nanomedicine: NBM* 2022;44:102577, https://doi.org/10.1016/j.nano.2022.102577

its early and accurate detection and diagnosis. Although early detection idea is currently being rigorously investigated, several fundamental and technical limitations remained to be overcome. Thus, the development of unconventional novel approaches is also persuaded to help more reliable diagnosis decisions.

Vibrational spectroscopies, IR and Raman, have long been investigated for cancer diagnosis from biopsy samples[6–17] However, due to the similarity in biomolecular composition of tissues, subtle spectral differences between healthy and cancerous tissue requires intensive data treatment to be able to demonstrate the differentiation. This becomes more of an issue as the cancer is at its early development. Therefore, the other modes of Raman Spectroscopy including Coherent anti-Stokes Raman spectroscopy (CARS),[18,19] Stimulated Raman spectroscopy (SRS),[20,21] and Surface-enhanced Raman Spectroscopy (SERS) have also been used to analyze biopsy samples for cancer diagnosis.[12–17] In a SERS experiment, a nanostructured noble metal, gold or silver, surface or colloidal particles are routinely used as substrates.[22–26] As it is obvious, intrinsic SERS spectra of a molecule, molecular composition or a biological structure can be used in label-free detection.

Despite all SERS-based studies with different tissue sampling methods has yielded important results for the analysis of cancerous tissues, there is no systematically developed SERS-based approach that can be easily integrated into routine clinical pathology settings. The disadvantages of working with fresh tissue, processing the tissue that takes time until the last stage, which includes the subjective interpretation of the pathologist, disrupting the structure of the tissue and causing uncertainty in the diagnosis could be avoided with a systematically developed SERS based approach. On the other hand, systematically optimizing a number of parameters of a SERS-based approach, from the surface on which the sample is placed, from the SERS active substrate to the optimization of the signal measurement parameters, will increase the applicability and reproducibility of the method. The literature is lacking in such a systematically optimized SERS-based approach.

In the study, it was aimed to develop a suitable surface for routine use to place the sliced tissue sample and allow the acquisition of SERS spectra without significant background interference. Thus, the cover glass slides were coated with polydimethylsiloxane (PDMS). Then, the cryosectioned tissue was placed on PDMS, before spotting the AgNPs colloidal suspension on the tissue. This approach is called as Cryosectioned-PDMS method. 31 normal and 33 abnormal pathologically evaluated tissue samples were obtained from thyroid disease patients to differentiate biopsied samples. The results demonstrate that the Cryosectioned-PDMS method is very effective in increasing the diagnostic accuracy with a simple sample preparation step promising the possible clinical translation of SERS into clinics for cancer diagnosis.

Methods

Preparation of SERS substrate

Solutions of silver nitrate ($AgNO_3$) (Sigma-Aldrich), hydroxylamine hydrochloride ($HONH_2{\cdot}HCl$) (Merck), and sodium hydroxide (NaOH) (Sigma-Aldrich) were prepared with double-distilled, deionized water from Millipore DirectQ-ultraviolet system. Leopold and Lendl based synthesis method to provide the synthesis of hydroxylamine reduced silver nanoparticles (h-AgNPs) was used.[27] Briefly, a total volume of 10 ml including 1.5×10^{2} M $HONH_2{\cdot}HCl$ and 3×10^{-2} M NaOH has added into 90 ml 1.11×10^{3} M $AgNO_3$ solution and stirred for 15 min at room temperature. The synthesized colloidal nanoparticles were characterized with Lambda 25, Perkin Elmer Ultraviolet-Visible (UV–Vis) spectrometer, and a JEOL 2100 Transmission Electron Microscopy equipped with an Oxford Instruments 6498 EDS system.

Preparation of PDMS covered glass substrate

Sylgard 184 silicone elastomer base and Sylgard 184 silicone elastomer curing agent manufactured by Dow Corning (Midland, MI). Sylgard 184 silicone elastomer base and Sylgard 184 silicone elastomer curing agent were used to produce the polydimethylsiloxane (PDMS) layer on the glass slide. PDMS substrates were made by directly mixing corresponding elastomer base and curing agent in a polystyrene beaker (base/agent mass ratio, 10:1). Then, 0.5 ml volume of the viscous gel was added into each six-well plate where the microscope glasses are cut and placed, which generates a 1.8 mm PDMS layer, found to be optimal thickness. The preparation of PDMS covered glass slides was completed after the plate was kept in an oven at 70 °C for 1 h.[28] For scanning electron microscopy (SEM) analysis, cross-sections from PDMS substrate were taken to measure the thicknesses. The SEM images were obtained by using a Carl Zeiss Evo 40 instrument under a high vacuum with a potential of 10 kV after coating with gold in a Polaron SC 502 sputter coater. Bovine liver tissue as a model was used in the optimization studies during the development of the approaches. Fresh bovine tissue samples were stored in a deep freeze at −80 °C until used for analysis.

Tumour samples

The biopsy samples of thyroid tissues were obtained from the patients with the consent of the ethical approval from Yeditepe University Hospital. The tissue specimens were stored at −80 °C in plastic tubes until the samples were prepared for the SERS measurements. After the tissue sample was removed from the deep freeze, it was thawed before placing on a cryostat chuck and embedded in an optimal cutting temperature compound (OCT) for cryostat sectioning. The OCT compound was purchased from PELCO®. Then, the tissue embedded in the OCT medium on chuck were left on the freeze bar of the cryostat. Cryostat chucks provide fast freezing of tissue specimens eliminating ice crystal formation (freeze artefact), which destroys cellular morphology. The frozen tissue was cryosectioned in desired thickness using a Shandon Cryotome SME Cryostat (Thermo Electron, UK) device.

Raman system and SERS measurement

SERS spectra of tissue specimen were collected using a Renishaw (Wotton-under-Edge, UK) InVia Reflex spectrometer equipped with a diode laser at 830 nm, CCD detector, edge filter,

holographic grating (1200 grooves/mm) with ultra-fast imaging Renishaw's StreamHR™ technology. The fast imaging mode, StreamHR with a high-speed encoded stage (HSES) and synchronized readout of the CCD detector were used in the mapping configuration and the Raman system was calibrated by using the silicon phonon mode at 520 cm^{-1} before SERS measurement. The incident laser power was adjusted to 30 mW on the sample and the spectral data acquisition time was 2 s for the Cryosectioned-PDMS method. SERS spectra over a spectral range of 582–1653 cm^{-1} (1100 cm^{-1} median value) were collected using the StreamHR point mapping acquisition method from a square grid of 10 × 10 scanned points from a total area of 22.5 μm × 22.5 μm (506.25 μm^2).

Data pre-processing and statistical analysis

Wire 4.1 software was used for pre-processing of the SERS data. First, cosmic ray removal was applied to each spectrum, and the SERS spectra were normalized to be equal to 1 before the data was used in classification algorithms. Baseline subtraction and smoothing method were only applied to visualize the differences in the spectral patterns on the plots but not used in the classification models means cosmic removed and normalized raw data with minimal preprocessing was used in the diagnostic classification algorithms. The pre-processed spectral dataset for statistical analysis was used in the statistical package for the social science (SPSS) package (SPSS Inc., Chicago, Illinois), which contains Principal Component Analysis (PCA), which is a data reduction technique that indicates the variations in a multivariate dataset, and Linear Discriminant Analysis (LDA) method to determine the variables that distinguish one group from the other by creating a discriminant function (DF) for each group. PCA was applied before LDA to reduce the number of dimensions in the original high-dimensional dataset and to derive the PC loadings, which indicates the directions and strength of variations of the selected parameters in the entire dataset. To apply PCA, the full range of SERS data having high predictors and specific regions of SERS data was placed into a data matrix using SERS spectra acquired for each method. The eigenvalue decomposition was performed on the covariance matrix of the spectral data matrix. The nineteen eigenvectors (eigenvalues greater than >1), were obtained, and the original spectral dataset was projected into the new coordinate system defined by the principal directions of variance, called the principal components (PCs), which are the linear combination of the original data variables.[29] Then, the first eight significant PCs vectors including 96.3 % of the variance related to the tissue specimen which demonstrated the highest classification rate were used to obtain regression (REGR) factors for classification the tissue specimens with PC-LDA. Leave one out-cross validation (LOO-CV) methodologies were applied to demonstrate the accuracy of the classification.[30]

Results

Characterization of nanoparticles

The synthesized colloidal suspension containing h-AgNPs was characterized using UV–Vis spectroscopy and TEM (Fig. 1A and C). The maximum absorbance of the UV–Vis

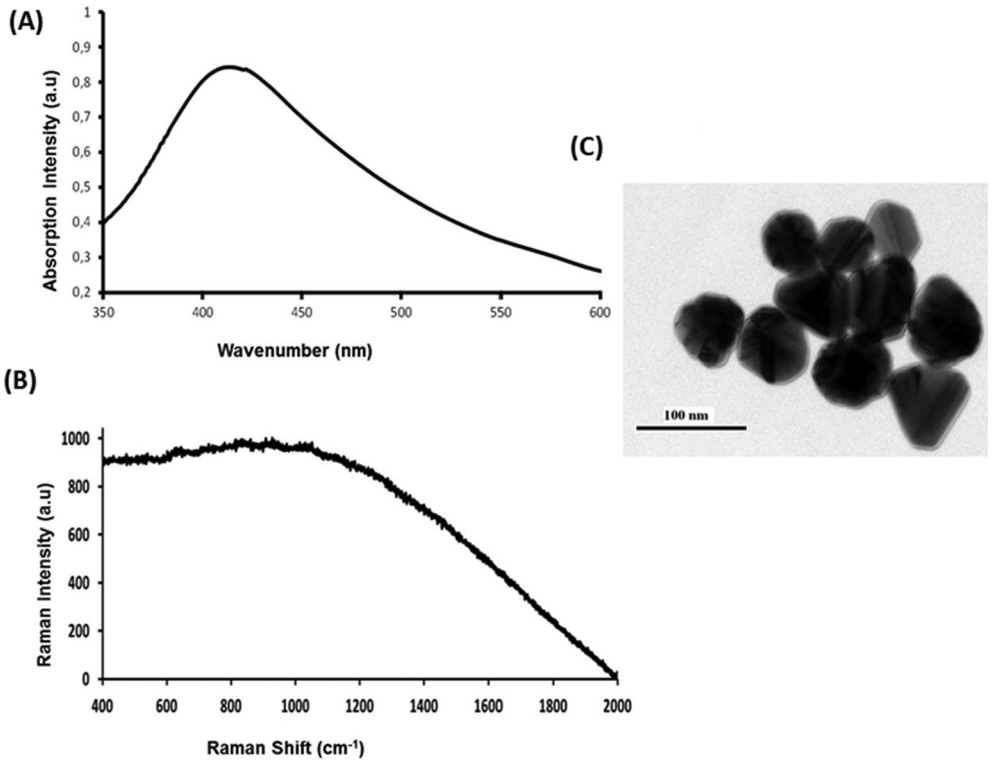

Fig. 1. Characterization of colloidal AgNPs. (A) UV–Vis spectrum. (B) A SERS spectrum of a colloidal suspension of AgNPs. (C) TEM image.

spectrum of the AgNPs colloidal suspension was observed at 413 nm, and the average diameter of the colloidal AgNPs was determined to be approximately 30 nm supported by TEM images. The final density of the AgNPs in the 16× concentrated suspension was calculated as 8.3×10^{11} particles mL.[31] A 20-μl volume of 16× colloidal AgNP suspension ($\approx 1.664 \times 10^{10}$ particles) was dropped on the CaF_2 substrate and left for drying at the suspended position. The SERS signal arising from the colloidal AgNPs was obtained with minimum spectral background coming from the suspension after a droplet of the suspension was placed on the CaF_2 slide (Fig. 1B).

Cryosectioned-PDMS method

Cryosectioned tissues specimen in 5-μm size were placed on the glass slide to facilitate the adaptation of the SERS technique into the clinic but the signal originating from the glass suppresses the scattering from the tissue. Therefore, a mould-casting method using PDMS to eliminate the background signal was used to cover glass slides. Fig. 2 shows the comparison of the spectra obtained from the same tissue sample on three different substrates where the tissue specimen was placed. As seen, the substrate where the tissue slice is placed has a dramatic effect on the spectra.

It was necessary to optimize the thickness of PDMS on the glass slide to prevent suppressing signals coming from the glass slide. Besides, to achieve optimal signal collection from sliced tissue, substrate thickness, tissue thickness, objective type, laser power, focus adjustment, acquisition type, number of spectra and mode, mapped area size, spectral range, drying configuration of droplet including AgNP suspension, AgNPs concentration, and region-dependent spectral reproducibility in the dried droplet area were also evaluated. Bovine liver tissue was used during the optimization studies. The details of experimental optimization for each parameter of the Cryosectioned-PDMS method was detailed in the thesis study[28] and a summary of the details of systematically optimized parameters during the development of the Cryosectioned-PDMS method was placed in the supporting information.

The following parameters were found to be optimal for the Cryosectioned-PDMS method. The thickness of the PDMS layer should be at least 1.8 mm to cover the glass slide to prevent the background. A 20 × objective and 830 nm laser with 30 mW power (as adjusted in the software) and 2 s exposure time were found to be suitable. The minimum thickness of the sectioned tissue to place on the glass slide should be 5-μm. The mapping of 10 × 10 points array using fast StreamHR method, using 16 × concentrated colloidal AgNPs suspension, and arranging the Raman shift range with a median value of 1100 (from ~580 to 1560 cm^{-1}) were necessary.

Comparison of substrate dependent signal reproducibility

The spectral reproducibility is an important factor, which is the key limitation of the SERS technique, due to the heterogeneity of the tissue structure and the chaotic (unpredictable) distribution of nanoparticles on the tissue surface. To increase the spectral reproducibility, it is necessary to obtain uniformly distributed colloidal AgNPs on a surface. The distribution of the AgNPs on the tissue placed on PDMS was more uniform compared to the distribution on the tissue placed onto CaF2 slide. Moreover, the substrate where the biopsy sample placed on were also optimized by comparing PDMS covered glass slide to CaF_2 substrate for their spectral reproducibility. For this comparison, the optimized experimental and instrumental parameters were applied to the tissue sections. The spot-to-spot and sample-to-sample reproducibility of the SERS spectra obtained by using PDMS and CaF_2 substrate platforms were utilized. In conclusion, the PDMS layers upon placing sliced tissue indicated a higher reproducibility compare CaF_2 slide (Table S1).

The distribution and packing of AgNPs aggregate on the tissue surface affect the signal reproducibility and quality as well. The suspended drying position of the droplet including colloidal AgNPs indicated an increased scattering and higher reproducibility in our previous studies.[32,33] The SEM images of suspended dried droplets including colloidal AgNPs on the cryosectioned tissue species placed on PDMS covered glass and CaF_2 slides were given in Fig. 3 as a comparison. To assess the distribution of AgNPs and their aggregates on the tissue surface, SEM images were obtained from the suspended dried droplet area including colloidal AgNPs. Fig. 3 shows the full SEM

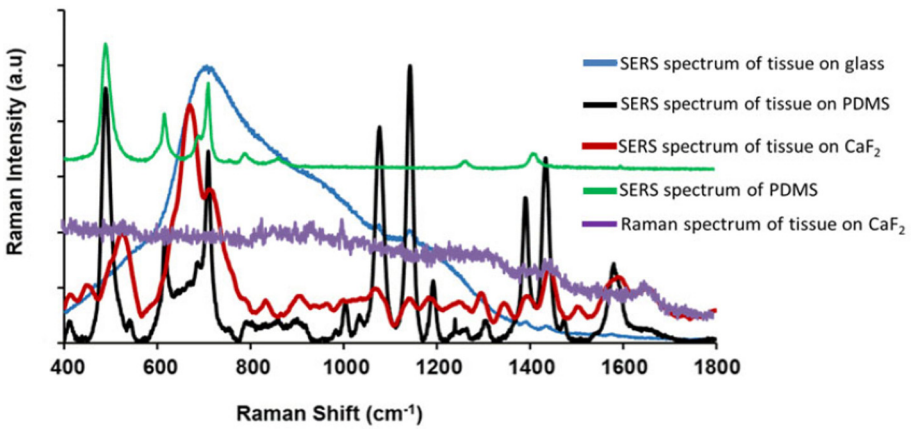

Fig. 2. SERS spectra of bovine liver cryosectioned tissue specimen placed on a glass slide, CaF_2 slide and PDMS layer with Raman spectrum of tissue placed on CaF_2 and SERS spectrum of PDMS.

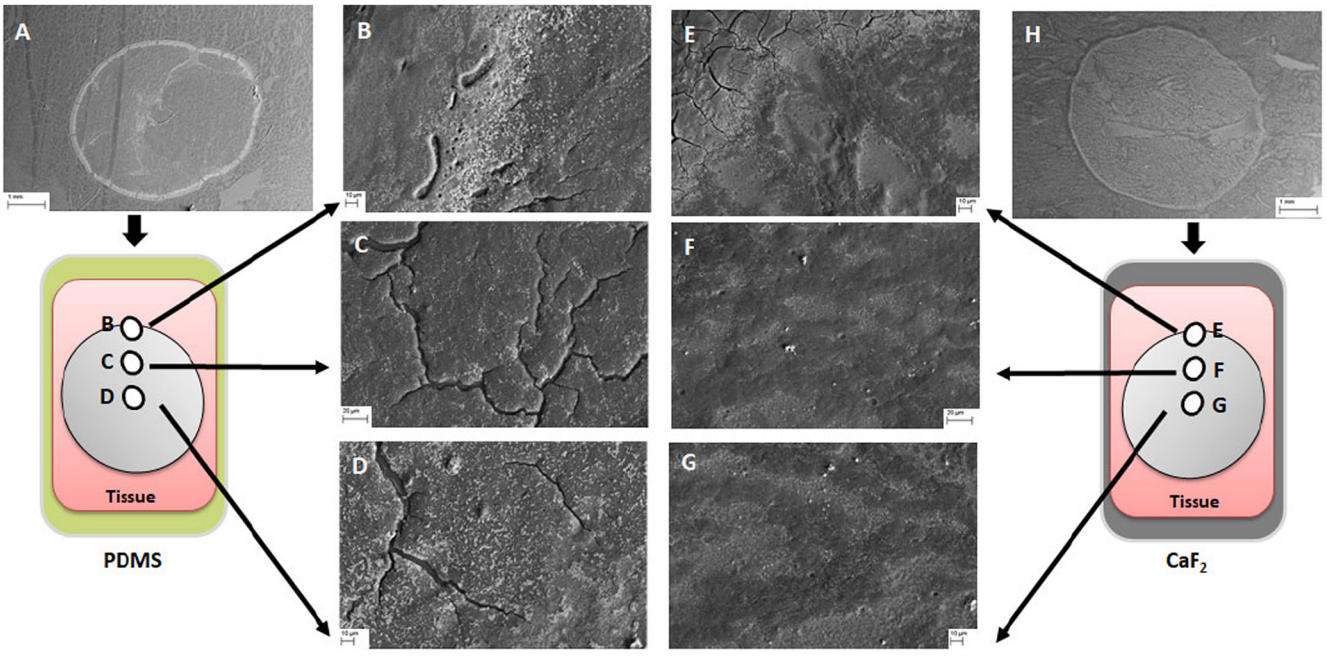

Fig. 3. SEM images of droplets placed on PDMS (A) and CaF_2 (H) and SEM images from three different regions on droplets of suspended dried droplet areas of colloidal AgNPs suspension on cryosectioned tissue surface placed on PDMS covered glass and CaF_2 slides. The first zoomed SEM image (B), the second (C) and the third (D) refer to the edge, in between and middle region of the suspended dried droplet on tissue specimen on PDMS. (E) SEM images of Edge, (F) in between, (G) middle region of a suspended droplet placed on tissue specimen on CaF_2. (Scale bars are respectively (A) 1 mm, (B)10-μm, (C) 20-μm, (D) 10-μm, (E) 10-μm, (F) 20-μm, (G) 10-μm, (H) 1 mm).

images of droplets and SEM images from three different regions for each droplet.

As seen, as a result of "coffee-ring" phenomenon, some of the AgNPs is packed at the edges while some are distributed through the droplet areas as single AgNPs or aggregates. The "coffee-ring" formation, which is a phenomenon that takes place in a drying droplet, and jams most of the particles at the liquid–solid–air interface.[34] When comparing SEM images, colloidal AgNPs for PDMS figuration appears to be denser, better dispersed and less agglomerated. This may be due to the difference in the hydrophobicity between the two surfaces. Therefore, reduced contact of the colloidal suspension with the more hydrophobic PDMS surface inside or outside the tissue sections may be the cause of improved reproducibility and signal quality.

Finally, the development of the Cryosectioned-PDMS approach for cancer detection with the final optimization was completed and this sampling approach was used for the classification of 64 biopsy samples involving 22 benign, 11 malignant and 31 healthy tissue samples. After the Cryosectioned-PDMS method was evaluated by its high reproducibility and high signal quality, it was applied on thyroid biopsy samples to provide a diagnostic classification among the malignant and benign tumours with healthy tissues by their SERS spectra regarding the biochemical information.

Diagnosis of thyroid tumours

SERS-based Cryosectioned-PDMS method was applied on 31 normal and 33 abnormal pathologically evaluated tissue samples obtained from 31 thyroid disease patients to different sample groups. Table S2 (Supplemental Material)shows the tissue type, collected spectra per sample and histopathological results of tissue specimen examined by the Department of Pathology, Fatih Sultan Mehmet Education and Research Hospital, University of Health Sciences. The tissue samples were marked as tumour (benign/malignant) and healthy (the tissue surrounding the tumour). Although the tissue surrounding the tumour is marked healthy and pathologically verified healthy, it might still have tumorous cells.

StreamHR point mapping acquisition from a square grid of 10 × 10 scanned points, a total area of 22.5 μm × 22.5 μm (506.25 μm^2), was performed with the optimized parameters of the Cryosectioned-PDMS approach. One hundred spectra per biopsy sample (a total of 6400 spectra for 64 biopsy samples) were collected.

The cosmic ray filtering, min-max normalization processes and smoothing through the WIRE.4.1 software of Renishaw's Raman System was applied to average spectra for each one hundred spectral data were estimated to represent each biopsy tissue specimen before using this multidimensional data (dimension = 64 × 1015) to construct loading vectors and regression (REGR) factors by using Principal Component Analysis (PCA) method. After the data processing, the average spectra were reduced into new relative variants called principal components scores (PCs). Ten significant PCs (eigenvalues greater than >1) were obtained by PCA method in the SPSS software as seen in Table S3 (Supplemental Material) in with the % value of explained variances in each PC. The PCs were evaluated using analysis of variance (ANOVA) to obtain significant PCs, and PC1, PC2, PC3, PC4, PC6, PC7 and PC8 loadings were used in

Linear Discriminant Analysis (LDA). The PC loadings indicating the significant variances in the malignant, benign and healthy tissue groups were illustrated in Fig. 4.

The scatter plots of PCA and PC-LDA analysis are shown in Fig. 5. The PCs of the first three factors were used in PCA scatter plot to visualize the variations among the averaged SERS spectra belonging to each biopsy specimen (Fig. 5A). The LDA classification algorithm to increase the classification accuracy by maximizing the differences within the groups was applied on PCs with the LOO-CV method obtaining a predicted classification result explained in the terms of sensitivity, specificity and accuracy. As a result, the PC-LDA scatter plot indicated well-classified groups among the benign, malignant and healthy biopsies as seen in Fig. 5B.

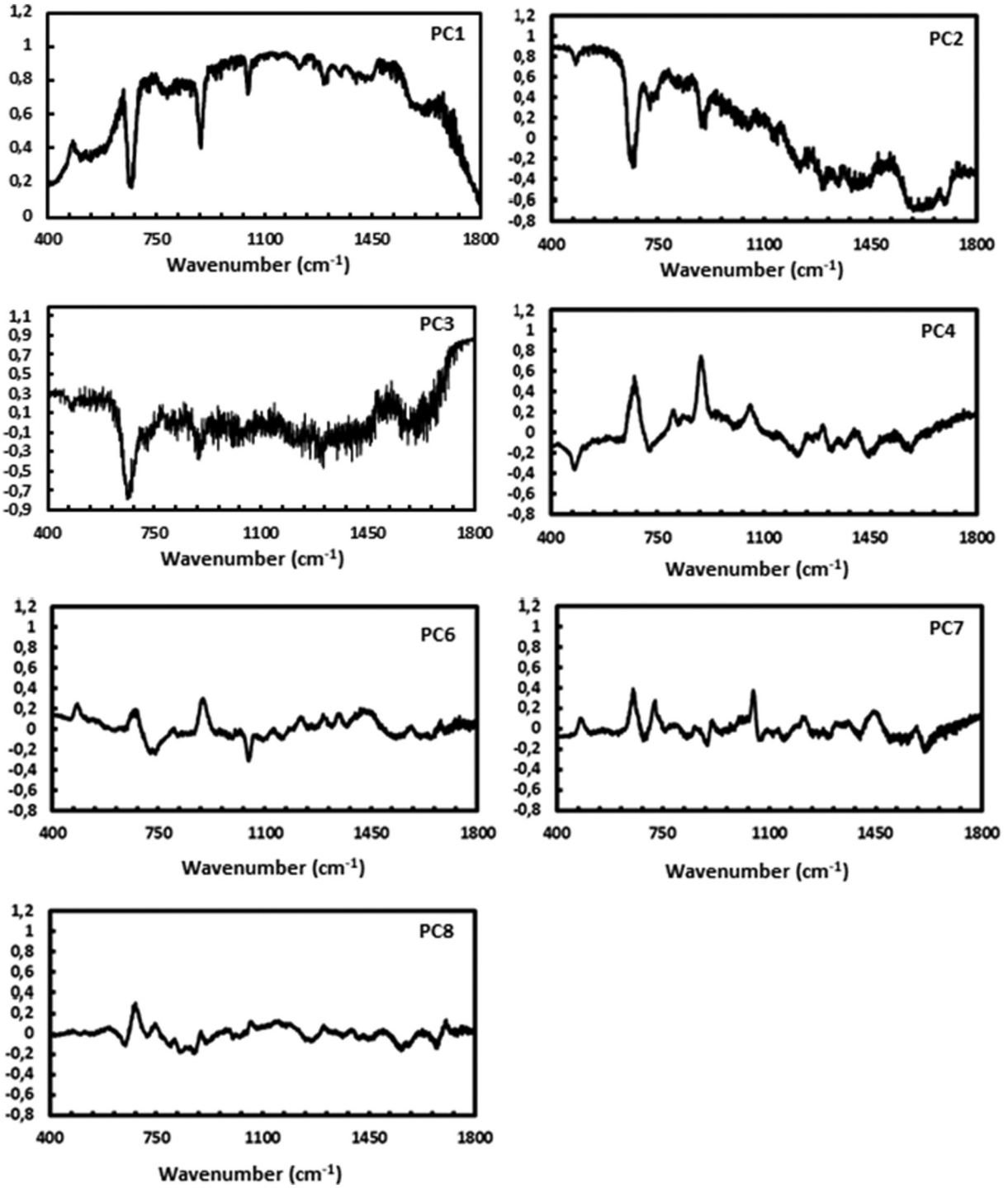

Fig. 4. The loadings of PC1 to PC4 and PC6 to PC8 for the spectral discrimination of malignant, benign and healthy tissue specimens.

The probability of correctly predicted performance of using PC-LDA classification algorithm with LOO-CV for differentiation of tumorous and healthy tissues resulted with the sensitivities of 94, 79 and 100 % and the specificities of 79, 71 and 77 %, and accuracy of 93, 76 and 91 % for by using the data set in the spectral range of 582 to 1563 cm^{-1} between benign and malignant; benign and healthy, malignant and healthy, respectively.

The PC1 and PC2 loading vectors extracted from the data using PCA to highlight the most prominent diagnostic variables among the spectra belonging to differently diagnosed tissue samples were shown in Fig. 6(A) with the average of SERS spectra obtained from malignant, benign and healthy tissue biopsies. The box-plot of Raman intensities of the healthy, benign and malignant groups at 656, 724, 740, 920, 960, 1048, 1096, 1328 and 1457 cm^{-1} in order to comprise the difference in SERS band intensities of malignant, benign and healthy tissue groups were shown in Fig. 6(B).

The mean SERS spectra of biopsied tissue specimens plotted with the PC1 and PC2 loading vectors explains the type of tissue from which the variations in band positions and intensities. PC 1 and PC 2 with positive as well as negative peaks in the same positions of the indicated biochemical elements display the most important features to differentiate malignant and benign tumours with healthy tissues.

The bands on the loading vectors can be attributed to biochemical components such as nucleic acids (724, 740, 1415 cm^{-1}), proteins (617, 667, 760, 920, 1008, 1052, 1180, 1280, 1295, 1315, 1334 and 1457 cm^{-1}), metabolites (724 and 920 cm^{-1}), and lipids (1096, 1385, 1435 and 1457 cm^{-1}), polysaccharides (1052 cm^{-1}) and mineral crystals (960 and 1052 cm^{-1}). The tentative assignments of the bands observed on the spectra of tissues are given in Table S4.[14,30,35–39]

The bands in the spectral range of 613 to 640 cm^{-1} can be attributed to the C—C twisting mode of phenylalanine or PDMS.[40] Therefore, this spectral range wasn't used in PC-LDA classification model. The bands in the spectral range of 667 to 675 cm^{-1}, 854 to 860 cm^{-1}, 1096 to 1100 cm^{-1} and 1382 to 1385 cm^{-1} can be assigned to C—S stretch frequencies of the cysteine residue in proteins, C—C backbone stretching vibrations, C—N stretch of lipids, and symmetric CH_3 stretching vibration of lipids, respectively.[38,39] SERS bands in the region of 724 to 732 cm^{-1} and 1334 to 1342 cm^{-1} can be assigned to ring breathing mode of DNA and RNA bases, and CH_3CH_2 wagging mode of collagen & polynucleotide chain (DNA purine bases), respectively.[37,40] The SERS bands in the region of 1002 to 1008 cm^{-1}, 1170 to 1180 cm^{-1} and 1278 to 1295 cm^{-1}, can be attributed to Phenylalanine, Tyrosine, and Amide III, respectively.[30,35,39,40] The SERS bands in the region of 1034 to 1065 cm^{-1}, can be assigned to the symmetric stretching vibration of $\nu_3PO_4^{3-}$ hydroxyapatite (HA) crystals, glycogen band (due to OH stretching coupled with bending or C—O stretching coupled with C—O bending of the C—OH groups or C—O stretching vibrations in protein, while the peak at around 920 and 960 cm^{-1} can be attributed to calcium phosphate apatite and lactic acid, respectively.[40,41] The major SERS bands in the region of 1397 to 1410 cm^{-1}, assigned to CH_2 deformation and the ester linkage C═O stretching vibrations in lipids and 1448 to 1452 cm^{-1}, assigned to CH_2 deformation in lipids.[42]

Then, the PC scores of each significant SERS bands at 667, 724, 740, 920, 960, 1052, 1096, 1315 and 1457 cm^{-1} instead of using the full spectral range obtained from the tissue samples were also evaluated in PC-LDA classification model. The derived factors were used in PC-LDA classification model with the LOO-CV method to obtain a predicted classification results. Table S5 shows the predicted classification results of PC components of specific spectral regions and full range of SERS data respective to malignant, benign and healthy tissues. The sensitivity, specificity and accuracy of classification results belong to healthy tissues and tumour biopsies was obtained high as 100 % using PC components of each specific spectral bands. The discrimination results of the diagnostic combinations of benign tumour versus malignant, benign tumours versus healthy tissues, and malignant tumours versus healthy tissues were achieved with the sensitivity, specificity and accuracy of 100, 95 and 97 %

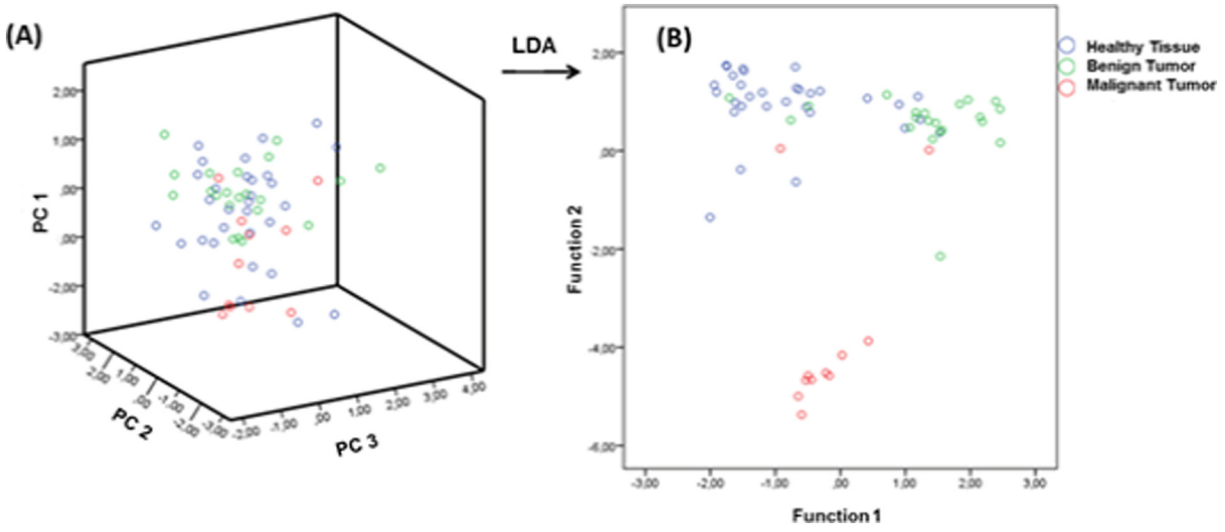

Fig. 5. Scatter plots of PCA (A) and PC-LDA (B) with the PC scores related to the spectra of healthy, benign and malignant tissues.

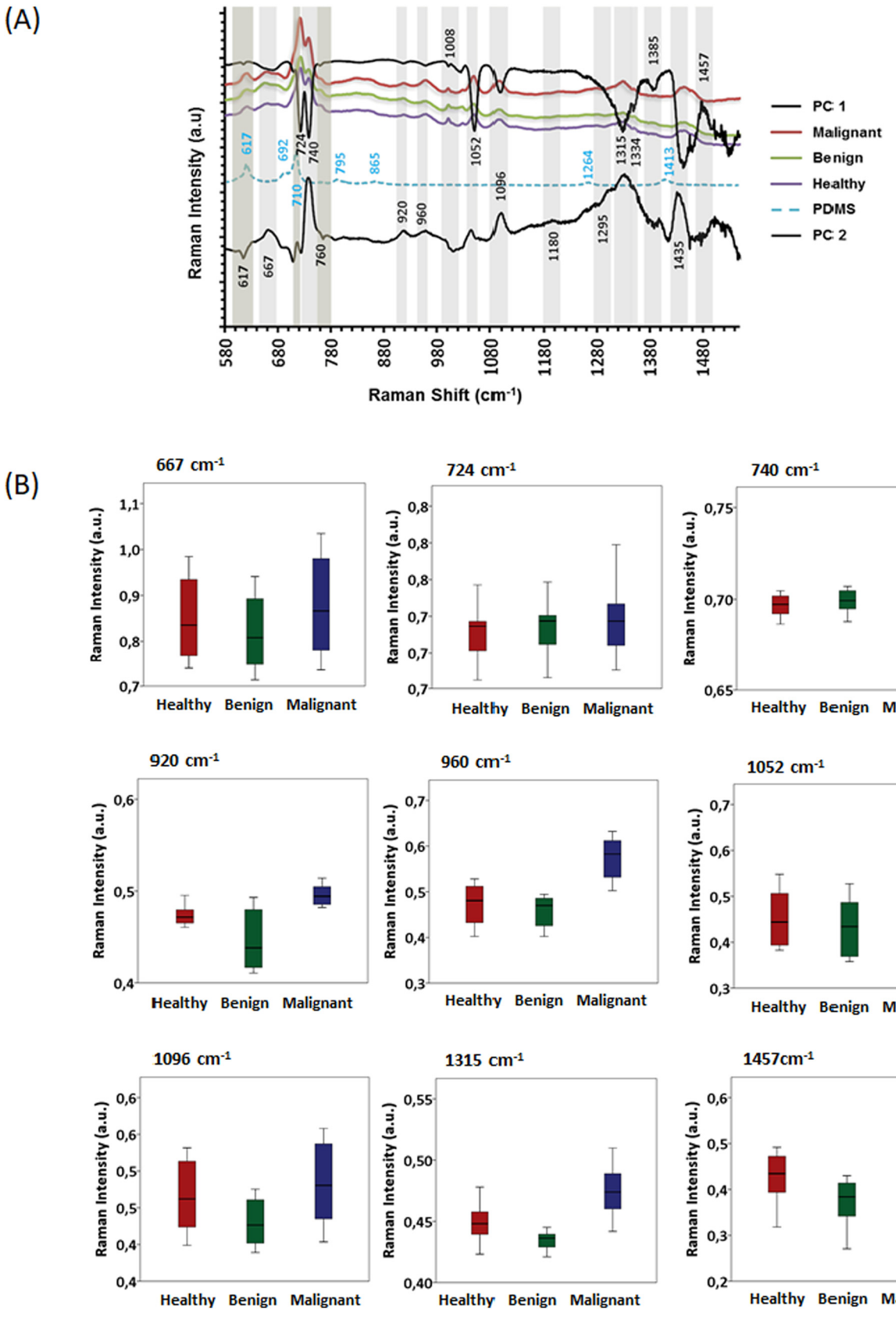

Fig. 6. (A) Mean SERS spectra of malignant (n = 11), benign (n = 22) and healthy (n = 21) tissue samples with the plot of the first two PCA loading vectors, PC 1 and PC 2 present the most important features to discriminate the normal and tumorous tissues of malignant and benign; (B) The box-plots of Raman intensities of the healthy, benign and malignant groups at 656, 724, 740, 920, 960, 1048, 1096, 1328 and 1457 cm^{-1}.

based on the PC components of SERS band at 740 cm^{-1} while the posterior probabilities based on the SERS band at 667, 724, 920, 960, 1052, 1096, 1315 and 1457 cm^{-1} was obtained achieved with the sensitivity, specificity and accuracy of 100, 100 and 100 %.

Discussion

Fine-needle aspiration biopsy (FNAB) is an effective method for the evaluation of thyroid nodules but the diagnostic accuracy of FNAB has been shown to be limited in large thyroid nodules.[43] In addition, biopsy results can sometimes cause delay in diagnosis, and the diagnosis of thyroid cancer by biopsy can be fraught with uncertainty due to sampling error or insufficiency.[1] Biopsy is costly and causes significant patient trauma.[44] All these issues highlight the urgent need for a time-saving and non-invasive method that can also provide much more accurate information to improve the diagnosis of thyroid diseases.

This SERS-based study presents a systematic approach that will help to translate the technique into clinics. The histology-based diagnosis includes several steps such as sectioning, mounting sectioned tissues on glass slide after fixation and embedding them into paraffin and staining. The presented study follows a similar procedure eliminating paraffin embedding and staining. Instead of staining, spectroscopic information is used for the evaluation of the disease status of the tissue sample. The study demonstrates the possibility of the use of more reliable biomolecular information for decision making by eliminating time consuming protocols and the possible artifacts during the sample preparation. This is why the tissue without fixation is studied with the snap-freezing method commonly used in molecular-based studies.[38,45] Recent Raman and SERS studies mainly used snap-frozen tissues without fixation and paraffin embedding due to the interfering peaks originating from paraffin wax at 1062, 1171–1175, 1130 and 1436 cm^{-1}. There is a systematic study performed in 2008 by a group of researchers demonstrating the effect of fixation processes on the Raman spectra.[46] In that study, different fixative agents were used to fix cells. Then, the spectral variances between fixated and unfixed cells were compared using classification models. The observations clarified that the fixation process affected the cell chemistry reflected by the spectral changes. Moreover, the classification accuracy was decreased in the fixated cells compared to unfixed cells leading to the misclassification of cancer and normal cells. Therefore, the frozen tissue samples without fixation and instead of paraffin-embedded was used in the study to avoid the proteome pitfalls for the realistic information from the SERS spectra of the environment of the biological tissue. On the other hand, the cryosectioned tissue slices in 5-μm thicknesses were used similar to the pathology routine in this study. The routine pathology laboratory uses glass slides to place tissue sections. This strong fluorescence background was aimed to eliminate by covering the glass with PDMS because it is a silicone-based elastomeric polymer with mechanical and chemical stability and is widely used in a variety of applications.[47,48] In addition, the type of SERS substrate is also important in a SERS measurement since it affects the quality of spectra. The AgNPs or AuNPs are routinely used in SERS experiments due to their simple preparation, low cost, and high enhancement effect.[49] The citrate reduced colloidal AgNPs are widely used as SERS substrates but it is difficult to synthesize without having anomalous peaks originating from the molecular debris formed during synthesis.[50] Thus, h-AgNPs was used due to having the benefits of increased reproducibility, minimal spectral background, high SERS activity and long-term stability, nearly 4 months.

In SERS and Raman studies, the spectral acquisition is usually carried out on quartz or CaF_2 slides because it has minimal background signal. However, these substrates are expensive and fragile materials. When working with tissue samples, large surface areas are needed. This systematic study concluded that PDMS-coated slides had a better signal quality than CaF_2 ones when the reproducibility of the SERS signals obtained from the droplet areas where the AgNPs are present on the cryosectioned tissue specimen. The possible reason is to be due to the fact that PDMS material is more hydrophobic than CaF_2 providing less chaotic distribution of AgNP aggregates on the droplet surface. After the suspension containing colloidal AgNPs was dropped onto the tissue sample on both substrates, it was observed that AgNP aggregates on CaF_2 surface were accumulated more at the edges of the dried droplet surface, whereas on PDMS it was more in the center and all over the surface (see Fig. 3). SERS signal reproducibility is a major concern of SERS studies, and because if the SERS active substrate is a colloidal suspension, the more uniform distribution of AgNPs is directly proportional to signal reproducibility. The SEM images show that AgNP deposits are less chaotic for PDMS than for CaF_2 and the distribution is denser on tissue samples providing increased uniform distribution of AgNP aggregates and increased signal reproducibility.

Whilst pre-processing of spectral data, though smoothing through the WIRE.4.1 software of Renishaw's Raman System was applied to the spectral data of malignant and healthy tissue specimen to visualize the band positions clearly in Fig. 4, original data without baseline correction was used in the PC-LDA classification models because variations in band intensity and localization could be appeared affecting the reliability of the results.

PCA was performed due to two primary reasons. The first one is to minimize high dimensional spectral data to new relevant scores to be able to use in LDA based diagnostic algorithm. The second one is to indicate the variability in the spectral data by extracted loading vectors, which represent the variances of each variable (wavenumber). The variations in the molecular components of tissue specimen were reflected on the spectra, and the variances can be observed by analyzing the loading vectors of the PCs with the positive and negative contributions related to the most important diagnostic vibrations in the spectra. The SERS bands at 656, 724, 740, 920, 960, 1048, 1096, 1328 and 1457 cm^{-1} observed in the mean spectra of the average spectra of each biopsied sample with the same diagnosis (Fig. 5(A)). Nevertheless, a slight shift of SERS bands at 656, 1001, 1048, 1328 and 1442 cm^{-1} to 667, 1008, 1044, 1315 and 1435 cm^{-1} respectively were observed on the loading PC vectors derived from the total SERS spectra of the tissue samples indicating the changes in peak position and relative peak amplitudes. PCA is also used as a sensitive diagnostic tool to observe the presence of peak position shift.[51]

The results of PCA loadings showed that the scattering of various vibrations in the malignant tissue differs markedly compared to the benign and healthy tissue, particularly in the region of nucleic acids (724, 740 and 1096 cm^{-1}), proteins (617, 1052, 1315 and 1457 cm^{-1}), lactic acid (920 cm^{-1}), and lipids (1385, 1435 and 1457 cm^{-1}), glycogen (1052 cm^{-1}), collagen (667, 1280 and 1334 cm^{-1}) and hydroxyapatite (960 and 1052 cm^{-1}). The peak at around 617 cm^{-1} exhibited on the PC 2 loading vector wasn't used in the PC-LDA classification model as it can be attributed not only to protein but to PDMS. In fact, the same laser power may be prevented from reaching the PDMS layer evenly below the 10 × 10 scanned points due to the heterogeneous tissue environment through the PDMS layer and cryosectioned tissue specimen for all biopsy samples were the same thickness used in the Cryosectioned-PDMS method.

The characteristic bands at around 724, 740 and 1096 cm^{-1} of the nucleic acids were observed more intense in the spectra of malignant tumours compared to benign tumours suggesting indicative of increased DNA and RNA metabolism in the thyroid cancer tissues because DNA and RNA metabolism are increased in proliferating cells compared to healthy cells.[52] Proliferating cells demand glucose which is converted to pyruvate through glycolysis.[53] However, there is a link between the increased glucose uptake of tumour cells and increased DNA/RNA metabolism. In proliferating cells, the glycolysis pathway is more used than the oxidative phosphorylation pathway because the production of ATP is more rapid.[54] This rapid production of ATP provides advantages for the survival and growth of tumour cells. The second reason is the provision of sufficient glycolytic intermediates to meet the biosynthesis needs of rapidly proliferating cells.[54] Glucose can also be used as a carbon source to produce ribose via the pentose phosphate pathway. Ribose-5-phosphate is then used to make RNA and DNA.[55] An additional feature of cancer cells is an increased rate of lipogenesis.[55] The newly synthesized lipids will be used for the synthesis of membranes and lipid-modified signal molecules, which explains the characteristic increased band intensity at 1385 cm^{-1} for malignant and benign tumours compared to healthy tissues. The results are in line with the metabolomic analysis of thyroid cancer (TC) tissues indicates increased glycolytic rate, lactate production and lipid biosynthesis.[56–58]

The spectra of fatty acids in the malignant tissue were dominated by the peak at around 1457 cm^{-1}, which is lower in the spectra of benign tissues compared to malignant and healthy tissues. The result of the lower intense peak assigned to the decreased fatty acid level in benign tissues was parallel with the result of the study exploring the thyroid malignancy by using Nuclear Magnetic Resonance and Gas Chromatography-Mass Spectrometry.[57] However, the band intensity referring to the fatty acid levels/ metabolism, which is higher in the spectra of malignant tissue compared to benign and healthy tissue, consists with the result of high levels of fatty acids observed in the malignant thyroid cells.[57]

The peak at around 920 cm^{-1} can be attributed to lactic acid, which is the prominent indicative of the Warburg effect due to the altered metabolism where cancerous cell tends to use glycolysis process instead of oxidative phosphorylation to generate energy because cancer cells require high bioenergy to promote and maintain cell growth.[58] Though the difference in the band intensity for malignant tissues compared to benign and healthy didn't appear much stronger, it has been observed higher in the spectra of malignant tissues.

Collagen assignment in the spectra at around 667 cm^{-1} is more intense for the tumorous tissues than healthy tissues. Collagen I is the most abundant extracellular scaffolding protein deposited in the tumour microenvironment and it is also associated with increased malignancy of tumours promoting migration, invasion and metastasis of cancer cells.[59–62] The peak at around 960 and 1052 cm^{-1} can be attributed to HA which is a naturally occurring mineral form of calcium apatite regarding calcifications in thyroids, as already mentioned, calcification signifies a risk of malignancy.[63] The study of integrative metabolites comparison in the malignant, benign and healthy thyroid tissues with the use of gas chromatography–mass spectrometry (*GCMS*) and *nuclear magnetic resonance* (*NMR*) has shown that Hypoxanthine contents are markedly increased in malignant lesions compared to benign lesions and benign lesions compared to healthy tissues.[57]

The protein profile assignment in the spectra of malignant tumours at around 1052, 1315 and 1457 cm^{-1} is observed more intense compared to benign tumours and healthy tissues. The increased levels of protein in malignant tissues can be due to maintaining the need for tumour growth.[56,57] The increased glycogen concentration in malignant tumours compared to benign tumours, which is another possible assignment in the spectra at around 1052 cm^{-1} is known as the clear cell change to differentiate benign and malignant tumours histologically.[64] It can be since benign tumours mostly grow slowly which metabolism is lower than cancerous cells even so some cases of fast-growing benign tumours was published.[65] Note that benign tumours are not classified as cancers because a benign tumour is a mass of cells lacking the ability to metastasize or locally invade tissue but it has the potential to become malignant through tumour progression.[66]

Conclusions

Each biopsy sample was cryosectioned in 5-μm size on the PDMS covered slides. Then, the SERS spectra were collected (spectral range was between 582 and 1563 cm^{-1} by given a median value of 1100 cm^{-1}) by using StreamHR fast point map acquisition method on a 10 × 10 points array (22.5 μm × 22.5 μm, scanned area size) from tissue surface after the droplet containing 20-μl volume from h-AgNP colloidal suspension was placed on the tissue surface and dried. Finally, the multidimensional data were reduced using PCA and used for training PC-LDA classification algorithm. The predicted results in PC-LDA model using LOO-CV method performing on the spectral data in the range of 582 to 1563 cm^{-1} for the diagnosis of 64 biopsy samples involving 22 benign, 11 malignant and 31 healthy tissue samples were obtained with sensitivities of 94, 79 and 100 % and the specificities of 79, 71 and 77 %, and accuracy of 93, 76 and 91 % for between benign and malignant; benign and healthy, malignant and healthy, respectively. However, the sensitivity, specificity and accuracy for the diagnosis of healthy and tumour biopsies using PCs coefficients of the bands at 667, 724, 920,

960, 1052, 1096, 1315 and 1457 cm^{-1} in LDA classification model were obtained as 100 % The proposed SERS based Cryosectioned-PDMS method would be a more effective and efficient analytical tool with higher diagnostic accuracy, simpler sample preparation steps and lower time for tissue analysis when compared to other existing spectroscopic methods and conventional methods used in the clinics today.

CRediT authorship contribution statement

Sevda Mert: Methodology, Validation, Formal analysis, Investigation, Resources, Writing – original draft, Writing – review & editing, Visualization, Project administration. **Seda Sancak:** Validation, Resources. **Hasan Aydın:** Validation, Resources. **Ayşe Tuba Fersahoğlu:** Validation, Resources. **Adnan Somay:** Validation. **Ferda Özkan:** Validation. **Mustafa Çulha:** Conceptualization, Methodology, Validation, Formal analysis, Investigation, Resources, Writing – original draft, Writing – review & editing, Visualization, Supervision, Project administration.

Declaration of competing interest

The authors have declared that no competing interest exists.

Appendix A. Supplementary data

Supplementary data to this article can be found online at https://doi.org/10.1016/j.nano.2022.102577.

References

1. McDougall IR, Berry GJ. *Management of Thyroid Cancer And Related Nodular Disease*. Springer; 2006.
2. Cooper D. American Thyroid Association (ATA) guidelines taskforce on thyroid nodules and differentiated thyroid cancer. Revised American Thyroid Association management guidelines for patients with thyroid nodules and differentiated thyroid cancer. *Thyroid* 2009;**19**:1167-214.
3. Gharib H, Papini E, Paschke R, Duick DS, Valcavi R, Hegedüs L, et al. American Association of Clinical Endocrinologists, Associazione Medici Endocrinologi, and European Thyroid Association medical guidelines for clinical practice for the diagnosis and management of thyroid nodules: executive summary of recommendations. *J Endocrinol Invest* 2010;**33**(5):287-91.
4. Udelsman R, Chen H. The current management of thyroid cancer. *Adv Surg* 1999;**33**:1-27.
5. Chiacchio S, Lorenzoni A, Boni G, Rubello D, Elisei R, Mariani G. Anaplastic thyroid cancer: prevalence, diagnosis and treatment. *Minerva Endocrinol* 2008;**33**(4):341-57.
6. Desroches J, Jermyn M, Pinto M, Picot F, Tremblay M-A, Obaid S, et al. A new method using Raman spectroscopy for in vivo targeted brain cancer tissue biopsy. *Sci Rep* 2018;**8**(1):1-10.
7. Bodanese B, Silveira FL, Zângaro RA, Pacheco MTT, Pasqualucci CA, Silveira Jr L. Discrimination of basal cell carcinoma and melanoma from normal skin biopsies in vitro through Raman spectroscopy and principal component analysis. *Photomed Laser Surg* 2012;**30**(7):381-7.
8. Desroches J, Lemoine É, Pinto M, Marple E, Urmey K, Diaz R, et al. Development and first in-human use of a Raman spectroscopy guidance system integrated with a brain biopsy needle. *J Biophotonics* 2019;**12**(3) e201800396.
9. Liu Y, Du Z, Zhang J, Jiang H. Renal mass biopsy using Raman spectroscopy identifies malignant and benign renal tumors: potential for preoperative diagnosis. *Oncotarget* 2017;**8**(22):36012.
10. Mackanos MA, Contag CH. FTIR microspectroscopy for improved prostate cancer diagnosis. *Trends Biotechnol* 2009;**27**(12):661-3.
11. Baker MJ, Gazi E, Brown MD, Shanks JH, Gardner P, Clarke NW. FTIR-based spectroscopic analysis in the identification of clinically aggressive prostate cancer. *Br J Cancer* 2008;**99**(11):1859-66.
12. Pirzada M, Altintas Z. Recent progress in optical sensors for biomedical diagnostics. *Micromachines* 2020;**11**(4):356.
13. Mert S, Özbek E, Ötünçtemur A, Çulha M. Kidney tumor staging using surface-enhanced Raman scattering. *J Biomed Opt* 2015;**20**(4)047002.
14. Feng S, Lin J, Huang Z, Chen G, Chen W, Wang Y, et al. Esophageal cancer detection based on tissue surface-enhanced Raman spectroscopy and multivariate analysis. *Appl Phys Lett* 2013;**102**(4)043702.
15. Li Z, Li C, Lin D, Huang Z, Pan J, Chen G, et al. Surface-enhanced Raman spectroscopy for differentiation between benign and malignant thyroid tissues. *Laser PhysLett* 2014;**11**(4)045602.
16. Czaplicka M, Kowalska A, Nowicka A, Kurzydłowski D, Gronkiewicz Z, Machulak A, et al. Raman spectroscopy and surface-enhanced Raman spectroscopy (SERS) spectra of salivary glands carcinoma, tumor and healthy tissues and their homogenates analyzed by chemometry: towards development of the novel tool for clinical diagnosis. *Anal Chim Acta* 2021;**338784**.
17. Aydin Ö, Altaş M, Kahraman M, Bayrak ÖF, Çulha M. Differentiation of healthy brain tissue and tumors using surface-enhanced Raman scattering. *Appl Spectrosc* 2009;**63**(10):1095-100.
18. Le TT, Huff TB, Cheng J-X. Coherent anti-stokes Raman scattering imaging of lipids in cancer metastasis. *BMC Cancer* 2009;**9**(1):1-14.
19. Legesse FB, Medyukhina A, Heuke S, Popp J. Texture analysis and classification in coherent anti-stokes Raman scattering (CARS) microscopy images for automated detection of skin cancer. *Comput Med Imaging Graph* 2015;**43**:36-43.
20. Yang Y, Yang Y, Liu Z, Guo L, Li S, Sun X, et al. Microcalcification-based tumor malignancy evaluation in fresh breast biopsies with hyperspectral stimulated Raman scattering. *Anal Chem* 2021;**93**(15): 6223-31.
21. Orringer DA, Pandian B, Niknafs YS, Hollon TC, Boyle J, Lewis S, et al. Rapid intraoperative histology of unprocessed surgical specimens via fibre-laser-based stimulated Raman scattering microscopy. *NatBiomedEng* 2017;**1**(2):1-13.
22. Fleischmann M, Hendra PJ, McQuillan AJ. Raman spectra of pyridine adsorbed at a silver electrode. *ChemPhysLett* 1974;**26**(2):163-6.
23. Jeanmaire DL, Van Duyne RP. Surface Raman spectroelectrochemistry: part I. Heterocyclic, aromatic, and aliphatic amines adsorbed on the anodized silver electrode. *J Electroanal Chem Interfacial Electrochem* 1977;**84**(1):1-20.
24. Aioub M, Kang B, Mackey MA, El-Sayed MA. Biological targeting of plasmonic nanoparticles improves cellular imaging via the enhanced scattering in the aggregates formed. *JPhysChemLett* 2014;**5**(15): 2555-61.
25. Zong C, Xu M, Xu L-J, Wei T, Ma X, Zheng X-S, et al. Surface-enhanced Raman spectroscopy for bioanalysis: reliability and challenges. *Chem Rev* 2018;**118**(10):4946-80.
26. Cialla-May D, Zheng X-S, Weber K, Popp J. Recent progress in surface-enhanced Raman spectroscopy for biological and biomedical applications: from cells to clinics. *Chem Soc Rev* 2017;**46**(13):3945-61.
27. Leopold N, Lendl B. A new method for fast preparation of highly surface-enhanced Raman scattering (SERS) active silver colloids at room temperature by reduction of silver nitrate with hydroxylamine hydrochloride. *J Phys Chem B* 2003;**107**(24):5723-7.
28. Mert S. *Development of SERS Based Methods for Early Cancer Detection*. Istanbul: Yeditepe University; 2018 [PhD].
29. Joliffe IT, Morgan B. Principal component analysis and exploratory factor analysis. *Stat Methods Med Res* 1992;**1**(1):69-95.

30. Molckovsky A, Song L-MWK, Shim MG, Marcon NE, Wilson BC. Diagnostic potential of near-infrared Raman spectroscopy in the colon: differentiating adenomatous from hyperplastic polyps. *Gastrointest Endosc* 2003;**57**(3):396-402.
31. Paramelle D, Sadovoy A, Gorelik S, Free P, Hobley J, Fernig DG. A rapid method to estimate the concentration of citrate capped silver nanoparticles from UV-visible light spectra. *Analyst* 2014;**139**(19): 4855-61.
32. Avci E, Culha M. Influence of droplet drying configuration on surface-enhanced Raman scattering performance. *RSC Adv* 2013;**3**(39): 17829-36.
33. Keskin S, Çulha M. Label-free detection of proteins from dried-suspended droplets using surface enhanced Raman scattering. *Analyst* 2012; **137**(11):2651-7.
34. Shen X, Ho C-M, Wong T-S. Minimal size of coffee ring structure. *J Phys Chem B* 2010;**114**(16):5269-74.
35. Feng S, Chen R, Lin J, Pan J, Wu Y, Li Y, et al. Gastric cancer detection based on blood plasma surface-enhanced Raman spectroscopy excited by polarized laser light. *BiosensorsBioelectron* 2011;**26**(7):3167-74.
36. Boca-Farcau S, Potara M, Simon T, Juhem A, Baldeck P, Astilean S. Folic acid-conjugated, SERS-labeled silver nanotriangles for multimodal detection and targeted photothermal treatment on human ovarian cancer cells. *Mol Pharm* 2014;**11**(2):391-9.
37. Liu Y, Huang L-q, Wang J, Tong H-m, Yuan L, Zhao L-h, et al. Fabrication of silver ordered nanoarrays SERS-active substrates and their applications in bladder cancer cells detection. *<sb:contribution><sb:title>Spectrosc Spectr</sb:title> </sb:contribution><sb:host><sb:issue><sb:series><sb:title>Anal</sb:title></sb:series></sb:issue></sb:host>* 2012;**32**(2):386-90.
38. Dai WY, Lee S, Hsu YC. Discrimination between oral cancer and healthy cells based on the adenine signature detected by using Raman spectroscopy. *JRaman Spectrosc* 2018;**49**(2):336-42.
39. De Gelder J, De Gussem K, Vandenabeele P, Moens L. Reference database of Raman spectra of biological molecules. *JRaman Spectrosc* 2007;**38**(9):1133-47.
40. Movasaghi Z, Rehman S, Rehman IU. Raman spectroscopy of biological tissues. *ApplSpectroscRev* 2007;**42**(5):493-541.
41. Rehman IU, Movasaghi Z, Rehman S. *Vibrational Spectroscopy for Tissue Analysis*. CRC Press; 2019.
42. Weinmann P, Jouan M, Dao NQ, Lacroix B, Groiselle C, Bonte J-P, et al. Quantitative analysis of cholesterol and cholesteryl esters in human atherosclerotic plaques using near-infrared Raman spectroscopy. *Atherosclerosis* 1998;**140**(1):81-8.
43. McCoy KL, Jabbour N, Ogilvie JB, Ohori NP, Carty SE, Yim JH. The incidence of cancer and rate of false-negative cytology in thyroid nodules greater than or equal to 4 cm in size. *Surgery* 2007;**142**(6):837-844. e3.
44. Zeiger MA. Distinguishing molecular markers in thyroid tumors: a tribute to Dr.Orlo Clark. *World J Surg* 2009;**33**(3):375-7.
45. Wang SS, Sherman ME, Rader JS, Carreon J, Schiffman M, Baker CC. Cervical tissue collection methods for RNA preservation: comparison of snap-frozen, ethanol-fixed, and RNAlater-fixation. *DiagnMolPathol* 2006;**15**(3):144-8.
46. Micke P, Ohshima M, Tahmasebpoor S, Ren Z-P, Östman A, Pontén F, et al. Biobanking of fresh frozen tissue: RNA is stable in nonfixed surgical specimens. *Lab Invest* 2006;**86**(2):202-11.
47. Fortuni B, Inose T, Uezono S, Toyouchi S, Umemoto K, Sekine S, et al. In situ synthesis of Au-shelled Ag nanoparticles on PDMS for flexible, long-life, and broad spectrum-sensitive SERS substrates. *Chem Commun* 2017;**53**(82):11298-301.
48. Paschoal AR, Costa NLM, Domingues RA, Santos EB. Fabrication of patterned small blocks of nanogold-loaded PDMS and its potential as reproducible SERS substrate. *Mater Lett* 2019;**255**126557.
49. Bonifacio A, Dalla Marta S, Spizzo R, Cervo S, Steffan A, Colombatti A, et al. Surface-enhanced Raman spectroscopy of blood plasma and serum using Ag and Au nanoparticles: a systematic study. *Anal Bioanal Chem* 2014;**406**(9):2355-65.
50. Larmour I, Faulds K, Graham D. SERS activity and stability of the most frequently used silver colloids. *JRaman Spectrosc* 2012;**43**(2): 202-6.
51. Ryu S-R, Noda I, Jung Y-M. Moving window principal component analysis for detecting positional fluctuation of spectral changes. *BullKorChemSoc* 2011;**32**(7):2332-8.
52. Lin D, Feng S, Pan J, Chen Y, Lin J, Chen G, et al. Colorectal cancer detection by gold nanoparticle based surface-enhanced Raman spectroscopy of blood serum and statistical analysis. *Opt Express* 2011;**19** (14):13565-77.
53. Muñoz-Pinedo C, El Mjiyad N, Ricci J-E. Cancer metabolism: current perspectives and future directions. *Cell Death Dis* 2012;**3**(1)e248-e.
54. Yu L, Chen X, Sun X, Wang L, Chen S. The glycolytic switch in tumors: how many players are involved? *J Cancer* 2017;**8**(17):3430.
55. Coleman PS. Membrane cholesterol and tumor bioenergetics. *Ann N Y Acad Sci* 1986;**488**:451-67.
56. Minuto MN, Shintu L, Caldarelli S. Proteomics, and metabolomics: magnetic resonance spectroscopy for the presurgical screening of thyroid nodules. *CurrGenomics* 2014;**15**(3):178-83.
57. Tian Y, Nie X, Xu S, Li Y, Huang T, Tang H, et al. Integrative metabonomics as potential method for diagnosis of thyroid malignancy. *Sci Rep* 2015;**5**(1):1-12.
58. Gill KS, Tassone P, Hamilton J, Hjelm N, Luginbuhl A, Cognetti D, et al. Thyroid cancer metabolism: a review. *JThyroid DisordTher* 2016;**5** (1).
59. Shintani Y, Maeda M, Chaika N, Johnson KR, Wheelock MJ. Collagen I promotes epithelial-to-mesenchymal transition in lung cancer cells via transforming growth factor–β signaling. *Am J Respir Cell Mol Biol* 2008;**38**(1):95-104.
60. Netti PA, Berk DA, Swartz MA, Grodzinsky AJ, Jain RK. Role of extracellular matrix assembly in interstitial transport in solid tumors. *Cancer Res* 2000;**60**(9):2497-503.
61. Ramaswamy S, Ross KN, Lander ES, Golub TR. A molecular signature of metastasis in primary solid tumors. *Nat Genet* 2003;**33**(1):49-54.
62. Armstrong T, Packham G, Murphy LB, Bateman AC, Conti JA, Fine DR, et al. Type I collagen promotes the malignant phenotype of pancreatic ductal adenocarcinoma. *Clin Cancer Res* 2004;**10**(21):7427-37.
63. Mathonnet M, Dessombz A, Bazin D, Weil R, Frédéric T, Pusztaszeri M, et al. Chemical diversity of calcifications in thyroid and hypothetical link to disease. *C R Chim* 2016;**19**(11–12):1672-8.
64. Garcia-Rostan G, Camp RL, Herrero A, Carcangiu ML, Rimm DL, Tallini G. β-Catenin dysregulation in thyroid neoplasms: down-regulation, aberrant nuclear expression, and CTNNB1 exon 3 mutations are markers for aggressive tumor phenotypes and poor prognosis. *Am J Pathol* 2001;**158**(3):987-96.
65. Sagel SS, Ablow RC. Hamartoma: on occasion a rapidly growing tumor of the lung. *Radiology* 1968;**91**(5):971-2.
66. Clark W. Tumour progression and the nature of cancer. *Br J Cancer* 1991;**64**(4):631-44.